Progress in Organic Coatings 185 (2023) 107928

Contents lists available at ScienceDirect

Progress in Organic Coatings

journal homepage: www.elsevier.com/locate/porgcoat

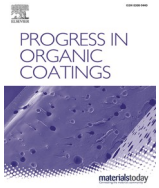

Improvement of the thermal efficiency of organic roof-coatings through design aimed at increasing the durability of thermochromic pigments

Massimo Calovi *, Alessia Zanardi, Stefano Rossi

Department of Industrial Engineering, University of Trento, Via Sommarive 9, 38123 Trento, Italy

ARTICLE INFO

Keywords:
Thermochromic pigments
Organic roof-coatings
Paint durability
Coatings thermal behavior
Long-term thermochromic efficiency

ABSTRACT

This work aims to improve the thermal efficiency of roof-coatings, by appropriate design of the samples. The pigments that provide thermochromic features to organic coatings, in fact, are susceptible to rapid physical-chemical degradation when exposed to atmospheric agents. Consequently, the study evaluated the effect of an additional top-layer with the task of increasing the durability and thermochromic efficiency of the pigments. The thermochromic pigment was analyzed by colorimetric analysis, infrared spectroscopy and optical and scanning electron microscope observations, while their thermochromic efficiency was evaluated exposing them to several thermal cycles. The protective properties of the coatings were assessed by electrochemical measurements, while their durability was investigated by different accelerated degradation tests. Finally, the thermal properties of the coatings were studied as a function of the degradation of the sample, to evaluate their thermochromic efficiency over time. This work demonstrates that the durability of the pigment, and consequently the thermochromic features of the coating, can be improved by applying an additional protective layer to the sample. Thus, this type of sample can be employed as roof-coating, with high long-term thermochromic efficiency.

1. Introduction

Since 1990, there has been an increasing trend in worldwide energy consumption [1], and recent research has estimated that global electricity consumption could more than double in the next 40 years [2]. Thus, the decrease in the dissipation of energy would be a key aspect for fighting pollution and the correlated climate change issues. Buildings are estimated to account for a third of the total amount of globally used energy and for a quarter of the total CO_2 emission [3], and 38 % of this energy consumption is employed for the functioning of Heating Ventilation and Air Conditioning (HVAC) systems [3]. To counter this tendency, the European Commission aims at reducing net greenhouse gas emissions by at least 55 % by 2030 [4]. Roofs are the main source of buildings heat storage, being exposed to direct solar radiation [5–7]. Materials able to improve the thermal properties of buildings exteriors, and especially of roofs, would thus greatly reduce the energy expenditure required for the HVAC systems [8–10].

'Smart' materials are defined as materials able to adapt and change their aspect in response to external stimuli [11,12]. They cover a wide range of applications: from the drug-delivery [13–15] and bioengineering sectors [16,17] to the realization of coatings able to assume different outlooks based on environmental conditions [18–20]. Among the 'smart' materials, thermochromic materials are particularly interesting, as they are able to change color state as a response to temperature fluctuations, in an irreversible or, more frequently, reversible manner [21,22]. The transition between two color states occurs thanks to an alteration in the equilibrium of molecules electrons, as a consequence of the received external stimulus [23]. A variety of oxides display thermochromic properties [24–26], which are employed to generate pigments used for the formulation of both thermochromic inks and polymers [27–29]. The thermochromic properties of a material are theoretically limitless, and not dependent on the number of color transitions [21], making this kind of material very attractive for a wide range of applications. Thermochromism is mostly applied in the textile industry [30–32], in the product packaging systems [33] and for the design of industrial machineries and kitchen tools [34], but also for the drawing of road markings [35,36] able to acquire a different coloration in case of icy conditions [35].

One of the most promising developments in this perspective is represented by the use of thermochromic coatings for the exterior of buildings. Thermochromic smart windows [37,38] have already been developed to improve the thermal indoor comfort [39]. As roofs are the

* Corresponding author.
E-mail address: massimo.calovi@unitn.it (M. Calovi).

https://doi.org/10.1016/j.porgcoat.2023.107928
Received 12 July 2023; Received in revised form 3 August 2023; Accepted 27 August 2023

external part of buildings mostly exposed to solar radiation, the employment of thermochromic roof coatings, able to change the color state upon temperature fluctuations, would offer further benefits. Different studies agree on the fact that thermochromic roof coatings may improve the energy efficiency of buildings [20,40–43] by absorbing solar energy at low temperatures and reflecting it at higher temperatures, thus reducing the need for heating and cooling systems [41]. Thermochromic roof coatings were shown to mitigate the so called 'urban heat islands' effect, with an improved thermal control inside buildings [44–46] with reduction in the use of energy and in the emissions of CO_2 [47,48]. To date, the major limitation to the outdoor application of thermochromic pigments is given by their poor chemical-physical resistance to external aggressive agents, and in particular to exposure to UV radiation [34,41,49,50]. Therefore, during the preparation of color-changing outdoor coatings some expedients are needed to prevent pigment degradation [49,51,52]. In addition to the weathering-induced degradation, another concern regarding the thermochromic efficiency of roof coatings is related to soiling due to environmental pollutants and dust. Indeed, when reflective materials are soiled, a reduction in the solar reflectance is observed [53], therefore reducing the desired thermal effect [54].

Therefore, the aim of the study is to improve the efficiency of thermochromic coatings, able to resist aggressive degradation conditions, thus suitable for outdoor uses. An additional clear-top coat layer was introduced in the design of the coatings, to provide protection and to enhance the thermochromic performances of the coatings. The thermochromic pigments were characterized by means of scanning electron microscope (SEM) and Attenuated Total Reflection (ATR) spectroscopy analyses, while the esthetical features of the coatings were assessed through color measurements. Moreover, the samples were exposed to the climatic chamber, and subjected to continuous temperature fluctuations below and above the color transition threshold, to evaluate the thermochromic efficiency of the pigments. The protective features of the coatings were investigated through electrochemical impedance spectroscopy (EIS) measurements, and their durability was assessed with accelerated degradation phenomena induced by exposure to UV-A and salt spray, and by fouling samples with soling agents. The protective contribution provided by the additional clear top-coat layer was evaluated during the conducted aging tests, monitoring the thermal behavior of the samples employing a specific lab-scale equipment.

2. Materials and methods

2.1. Materials

The thermochromic pigments were supplied by SFXC (Newhaven, UK) and used as received. When heated above 28 °C, they turn from "black" to "transparent" colors. The process is totally reversible following cooling and reheating. The 10,466 IR Black chromium green-black hematite dark brown pigment was provided by Vibrantz Technologies (Mayfield Heights, OH, USA). Acetone, Fe_2O_3, NaCl, $CaSO_4$ and humic acid were purchased from Sigma-Aldrich (St. Louis, MO, USA) and used as received. The $NaNO_3$ reagent was purchased from J.T Baker (Phillipsburg, NJ, USA). The carbon steel substrate (Q-panel type R (0.15 wt% C - Fe bal.) - 40 mm × 70 mm × 2 mm dimensions) was provided by Q-lab (Westlake, OH, USA). The waterborne 2 K acrylic-based white primer paint ECOFILLER EQW and the waterborne 2 K polyurethane-acrylate transparent top-coat paint IDROPUR ZW 01 were supplied by EP Vernici (Solarolo, Ra, Italy).

2.2. Samples production

The carbon steel substrates were appropriately pre-treated before to painting in order to enhance the coating's adherence. The metallic panels were initially degreased with an ultrasound treatment in acetone for 2 min. Thus, the mechanical pickling was completed employing a sandblasting procedure with corundum powder (0.2 mm diameter - 70 mesh), delivering the steel substrates a roughness [Ra] of 3.24 ± 0.13 μm. Finally, an additional acetone degreasing procedure was carried out to eliminate any potential contamination traces.

Three sets of samples were produced and characterized in this work, as summarized in Table 1. Each of them was made up of a spray-applied first layer of white acrylic-based primer. The samples were allowed to cure in an oven at 60 °C for 30 min prior to the succeeding top-coat application.

Subsequently, a top-coat layer was applied to the samples, modifying the formulation of the polyurethane-acrylate transparent paint by adding the specific amount of black pigment in sample B and thermochromic pigment in samples T and TT. The paint mixtures were mechanically mixed for 30 min prior to application, to guarantee the uniform distribution of the pigments in the polymeric matrix. However, as thermochromic pigments are known to suffer upon exposure to UV radiation, an additional clearcoat layer made by the polyurethane-acrylate transparent paint was applied on sample TT, with the aim of increasing the durability of the thermochromic properties of the coating. In fact, as the acryl-polyurethane paint is based on water-soluble acrylic modified resins and aliphatic isocyanate, it is not susceptible to UV exposure.

Therefore, sample B was used as a reference during the various characterization tests, representing a standard black coating devoid of thermochromic features. On the other hand, sample TT was produced in an attempt to enhance the thermochromic functions of the pigments over time, comparing their performance with those of sample T.

2.3. Characterization

The low vacuum scanning electron microscope SEM JEOL IT 300 (JEOL, Akishima, Tokyo, Japan) was employed to assess the morphology of the thermochromic pigment, while the optical stereomicroscope Nikon SMZ25 (Nikon Instruments Europe, Amstelveen, the Netherlands) was used to highlight their temperature dependent aesthetic features. Moreover, FTIR infrared spectroscopy measurements were acquired in attenuated total reflection (ATR) mode with a Varian 4100 FTIR Excalibur spectrometer (Varian Inc., Santa Clara, CA, USA), to investigate the chemical composition of the thermochromic pigment.

SEM observations were also employed to analyze the morphology of the coatings, with the aim of verifying the compatibility between the polymeric matrix and pigment. Thus, the aesthetic feature of the coatings was evaluated with a Konica Minolta CM2600d spectrophotometer (Konica Minolta, Chiyoda, Tokyo, Japan), using a D65/10° illuminant/observer configuration in SCI mode.

The protective properties of the coatings were assessed with Electrochemical Impedance Spectroscopy (EIS) measurements, using a potentiostat Parstat 2273 (Princeton Applied Research by AMETEK, Oak Ridge, TN, USA) with the software PowerSuit ZSimpWin (version 2.40) and applying a signal of about 15 mV (peak-to-peak) amplitude in the 10^5–10^{-2} Hz frequency range. The cell setup was med of an Ag/AgCl reference electrode (+207 mV SHE) and a platinum counter electrode, immersed in the 3.5 wt% sodium chloride aqueous solution. The samples were kept immersed in the test solution for a total of 7 days, analyzing a testing area equal to 6.5 cm^2. The measurements were carried out on five samples per series.

Table 1
Samples nomenclature.

Sample	First layer	Second layer	Third layer
B	White primer	Top-coat +5 wt% black pigment	/
T	White primer	Top-coat +5 wt% thermochromic pigment	/
TT	White primer	Top-coat +5 wt% thermochromic pigment	Clearcoat

Thus, the durability of the samples was investigated by means of different accelerated degradation tests. The samples were exposed in a climatic chamber ACS DM340 (Angelantoni Test Technologies, Perugia, Italy), to evaluate the long-term efficiency of the thermochromic reversibility of the pigment and the coatings. The temperature values were alternated between 20 °C and 40 °C, for a total of 1500 cycles. As the color transition temperature (28 °C) lies in between, during the test the thermochromic pigment was forced to move from the black state to the colorless state 1500 times. The thermochromic properties during the climatic chamber test were assessed through color change measurements and by recording the time for the sample surface to completely change color upon heating.

Furthermore, the samples were characterized with the experimental setup schematized in Fig. 1, adapted from previous studies [55–58], to evaluate the effect of the thermocromic pigment on the thermal behavior of the coatings. The testing setup involved a roof panel-sized coated sample measuring 150 × 150 × 2 mm^3 that was placed on a roofless box measuring 200 × 270 × 200 mm^3 composed of polyurethane foam sheets. The sample under investigation was exposed to a 150 W IR-emitting lamp (Philips IR150R R125, Eindhoven, Netherlands) placed at a distance of 260 mm. A thermocouple PT 100 (temperature sensor) was located beneath the coating panel, to evaluate the temperature transmitted by the panel inside the structure, defined as T_{surf}. The thermocouple was connected to a Delta OHM HD 32.7 RTD (Delta OHM Srl, Selvazzano Dentro, Italy) data logging instrument and the temperature data were recorded every 5 s. The instrument was controlled by DeltaLog 9 software. The temperature evolution under the IR lamp irradiation has been recorded by the thermocouples until a plateau was reached (20 min). Thus the external surface temperature of the panels T_{ext} was assessed employing an IR-camera FLIR T62101 (FLIR, Milan, Italy). The IR-images were acquired 240 mm in front of the house model set-up, approximately in correspondence of the thermocouple. The emittance of each sample was assumed to be 0.95.

The long-term efficiency of the coatings was evaluated interspersing each thermal measurement with an accelerated degradation cycle according to the ISO 20340:2009 standard [59], composed of:

- 72 h of alternate cycles of 4 h exposure to UV-A (340 nm) at (60 ± 3) °C and 4 h exposure to condensation at (50 ± 3) °C, employing an UV173 Box Co.Fo.Me.Gra (Co.Fo.Me.Gra, Milan, Italy) and following the ISO 11507:1997 [60];
- 72 h of exposure in salt spray chamber (Ascott Analytical Equipment Limited, Tamworth, UK), in accordance with ISO 7253:1996 [61];
- 24 h at room temperature.

The thermal performance and aesthetic qualities of the samples were determined after each degrading cycle. Moreover, FTIR infrared spectroscopy measurements were used to observe any potential chemical decay of the coatings. Furthermore, to better explain the evolution of the thermal performance of the coatings, the pigments alone were exposed to UV-A radiation for 100 h, analyzing their physical-chemical degradation with SEM observations and evaluating their residual thermochromic efficiency by means of colorimetric analysis.

Finally, to determine the influence that soiling may have on the thermochromic properties of pigments and coatings, the accelerated soiling and weathering test was conducted according to the ASTM D7897/18 standard [62], using a soiling mixture that simulates the Miami climate (hot and humid). The soiling mixture was prepared employing the following compounds:

- Dust: a mixture of 0.3 g of iron oxide Fe_2O_3 powder (CAS 1309-37-1), 1.0 g of montmorillonite K10 powder and 1.0 g of bentonite, which were transferred to 1 L of distilled water (suspension of 2.3 g/L).
- Salts: a mixture of 0.3 g of sodium chloride NaCl, 0.3 g of sodium nitrate $NaNO_3$ and 0.4 g of calcium sulfate dihydrate $CaSO_42H_2O$, which were transferred to 1 L of distilled water (solution of 1.0 g/L).
- Particulate organic matter (POM): 1.4 g of humic acid (CAS 1415-93-6) diluted in 1 L of distilled water (solution of 1.4 g/L).
- Soot: 0.26 g of carbon black (Vulcan XC-72) diluted in 1 L of distilled water (solution of 0.26 g/L).

Thus, the samples were subjected to 3 stages of degradation test:

- Weathering: apparatus exposure before soiling: 2 cycles, each of them composed of 8 h in UV-A chamber and 4 h of water condensation at 50 °C and a final dry under the infrared lamp;
- Soiling: spray the mix of dust, salts, organic matter and soot and dry under the infrared lamp;
- Weathering: apparatus exposure after soiling: 2 cycles, each of them composed of 8 h in UV-A chamber and 4 h of water condensation at 50 °C and a final dry under the infrared lamp.

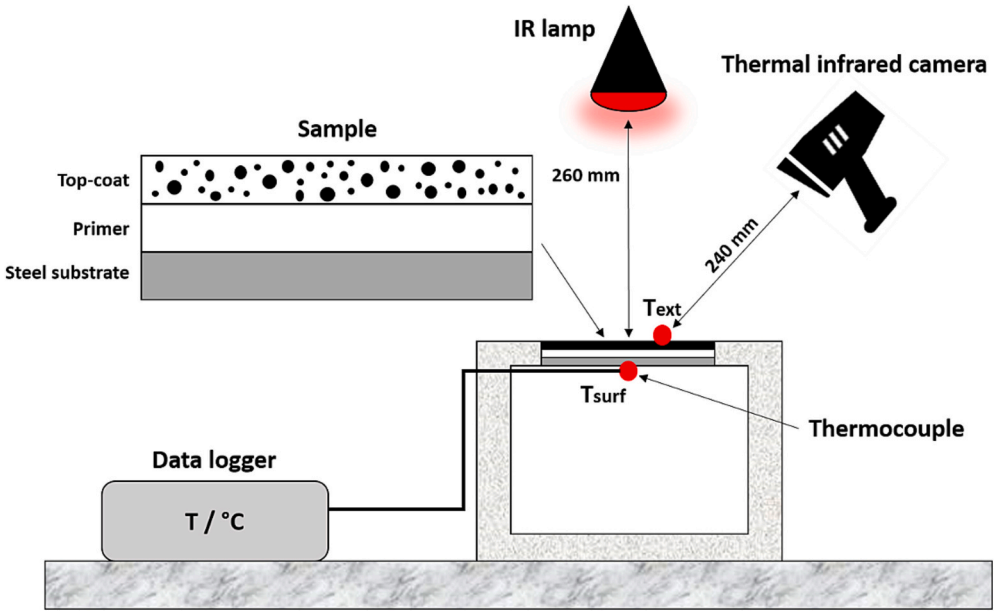

Fig. 1. Experimental set-up employed for the thermal behavior measurements performed with the IR emitting lamp.

The weathering steps were performed employing an UV173 Box Co. Fo.Me.Gra, while the soiling mixture was sprayed above the sample. Finally, the samples were dried under a 150 W IR-emitting lamp (Philips IR150R R125) for 15 min. The thermal properties of the coatings were then assessed by measuring the external and surface temperatures, employing the setup depicted in Fig. 1.

3. Results and discussion

3.1. Pigments characterization

Fig. 2 exhibits the SEM micrograph of the thermochromic pigment, which is composed of spherical particles with a diameter <10 μm, mainly constituted of carbon and oxygen, as revealed by the EDXS elemental analysis. The presence of spherical particles in the composition of thermochromic pigments has been already detected in previous studies [49,51]: indeed, the thermochromic properties of these pigments lie in the ability of the spherical particles to change from a colored state to a colorless condition at the transition temperature of 28 °C. In this specific case, beneath the threshold temperature of 28 °C the pigments appear as black, while above 28 °C they turn transparent.

Fig. 3 reveals the appearance of the thermochromic pigment observed with the optical stereomicroscope in the cold state, below the color transition temperature of 28 °C (Fig. 3a), and at higher temperature (Fig. 3b). The powders were placed on a red colored support, to better appreciate their chromatic change as a function of the applied temperature. The two images highlight the relevant color transition of the spherules from the black to the transparent state above the threshold temperature of 28 °C.

Typically, thermochromic pigments consist of 3 different components, each of which plays a specific role:

- the color precursor, which supply the pigment with its fundamental color;
- the color developer [41,63], which confers the color shift *via* electron acceptance/donation interactions with the color precursor [64];
- the solvent, able to regulate the transition temperature with its melting point, promoting component migration [41,63].

This blend is enclosed in microcapsules, similar to the spherical structures of the thermochromic powder characterized in this work, which must ensure the proper functioning of the pigments [21,41,63].

Thus, the ATR infrared spectroscopy was exploited to investigate the molecular composition of the thermochromic pigment. The ATR spectrum is displayed in Fig. 4. The peaks obtained with the IR analysis match with the ATR spectra of the 6(diethylamino)-1,2benzofluoran and the oxydiphenol molecules [63]. Specifically, the peaks at 2915 cm^{-1} and 2847 cm^{-1} are associated with the stretches of the C—H groups of the compounds. The signals at 1737 cm^{-1} and 1551 cm^{-1} are instead linked to the C═O functional groups and the bending of the N—H bond of the dyethylamino-benzofluoran, respectively. The absorption band at 1462 cm^{-1} is due to the aromatic region of the oxydiphenol, while the peak at 1343 cm^{-1} corresponds to the amine functional groups. The signal at 1172 cm^{-1} corresponds to the oxydiphenol C—O functional group. Eventually, the intense peak at 811 cm^{-1} is linked to the C—H bonds of the aromatic regions out of the plane bend, present in both the diethylamino-benzofluoran and the oxydiphenol molecules.

Given the ATR results, it is possible to speculate that the spherical particles constituting the pigment are composed of a combination of 6 (diethylamino)-1,2benzofluoran and oxydiphenol. These two molecules are already known to be responsible for the thermochromic properties of other chromogenic pigments [49]. The presence of 6(diethylamino)-1,2benzofluoran and oxydiphenol in the spherules will thus determine the black color of the pigment at low temperatures, and its transparency at higher temperatures.

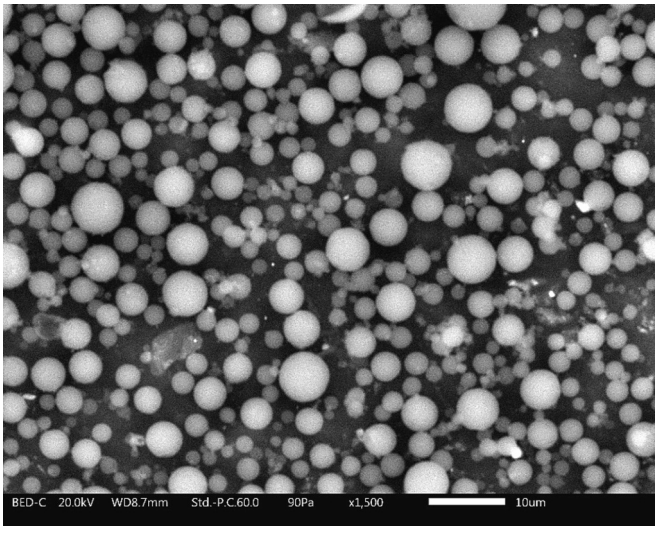

Fig. 2. SEM micrographs of thermochromic pigments.

3.2. Coatings morphology and aesthetical features

The average thickness values of layers composing the coatings are reported in Table 2.

Fig. 5 shows the SEM micrographs of the cross-sections of the three sample typologies. The primer layer is equal for all the samples, and possesses a thickness of about 60 μm. Sample B and sample T have a pigmented top-coat of thickness of about 40 μm and 100 μm, respectively. The different thickness of the two top-coats, made up of the same paint, is probably caused by the different molecular composition of the two pigments (black for sample B and thermochromic for sample T), which modify the rheology of the polymeric matrix and the yield of the spray deposition. Rather than controlling the uniformity of the thicknesses of the coatings using alternative deposition techniques, such as the use of a film spreader, the various layers were applied by spray, as it is one of the simplest and most used processes in the industrial sector. This choice has made it possible to highlight the impact of the addition of pigments on the yield of the spray deposition process. With this consideration, during all the deposition processes, the same amount of material was applied per single deposition, equal to about 0.125 L/m^2, as specified by the paint manufacturer, observing however considerable changes in the thicknesses of the second layer between the three series of samples B and T/TT. The layers containing the thermochromic pigments are clearly visible in Fig. 5b and Fig. 5c, as they present the spherules (dark in color) homogeneously dispersed within the polymeric matrix. Finally, sample TT sample has a further transparent layer, about 60 μm thick, which makes its coating the thickest of all, equal to about 210 μm. Consequently, the three samples possess coatings with different overall dimensions: this aspect can have a non-negligible impact on their protective and durability performance.

Fig. 6 represent the surface of the as-prepared samples in the cold state and in the hot state, above the threshold temperature of color transition (28 °C). Sample B, devoid of thermochromic pigments, does not exhibit any temperature-dependent color variation. Differently, the surface of samples T and TT appears white at high temperatures. Indeed, the paint applied for the top-coats is transparent and the thermochromic pigment appears as colorless above the color transition temperature. Thus, the overall appearance of the surface of the two samples is determined by the color of the underlying primer layer, which is actually white. Moreover, since the appearance of the samples T and TT is very similar in both thermal states, the additional clearcoat in the sample TT does not significantly affect the aspect of the coating.

Table 3 reports the colorimetric coordinates of the samples, according to the CIE-L*a*b* method [65]. Accordingly, a color is described

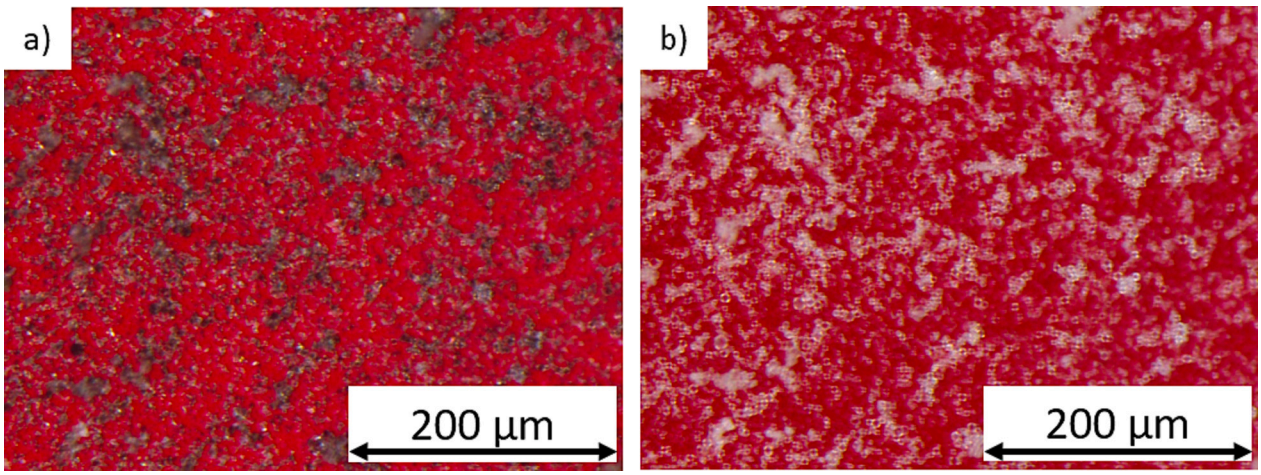

Fig. 3. Optical stereomicroscope micrographs of the thermochromic pigment: (a) below the color transition temperature of 28 °C and (b) over the transition temperature value.

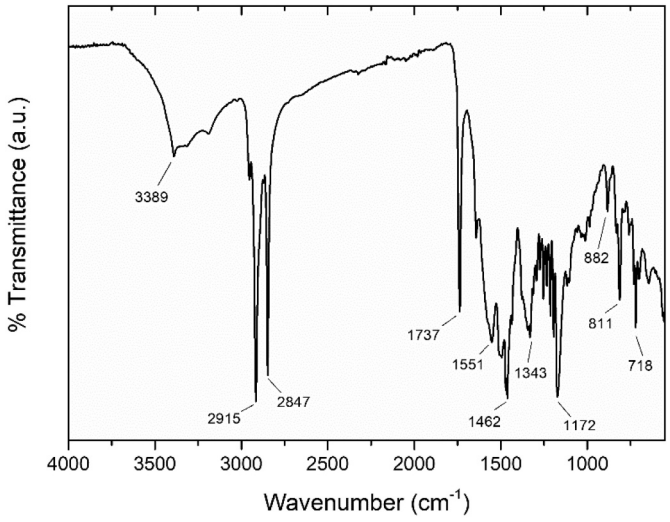

Fig. 4. ATR spectrum of the thermochromic pigment.

Table 2
Coatings thickness.

Sample	First layer (µm)	Second layer (µm)	Third layer (µm)	Total coating (µm)
B	≈ 60	≈ 40	/	≈ 100
T	≈ 60	≈ 100	/	≈ 160
TT	≈ 60	≈ 90	≈ 60	≈ 210

by three coordinates: L*, the lightness, goes from 0 (black) to 100 (white); a* indicates the red-green coordinate (a* > 0 for red and a* < 0 for green); b* indicates the yellow-blue scale (b* > 0 for yellow and b* < 0 for blue) [66,67]. As confirmed by the images in Fig. 6, the color coordinate values of samples T and TT are comparable in both the cold and hot states. In contrast, sample B, which contains a different pigment, shows slightly distinct color coordinate values, resulting in an overall divergence in appearance in the cold state, compared to the two thermochromic coatings.

Thus, the color change ΔE of the samples between hot and cold state was calculated as a function of the three color coordinates, to evaluate the impact of thermochromic pigments on the appearance of the coatings. The value of ΔE was computed, according to the ASTM E308–18 standard [66], as follow:

$$\Delta E = \left[(\Delta L^*)^2 + (\Delta a^*)^2 + (\Delta b^*)^2\right]^{1/2}.$$

The consequent color change between the cold state and the hot state is reported in Table 4. As samples T and TT change from a dark black color to white, the value of ΔE value provoked by the thermal change reaches 57–58 points, demonstrating a significant visual variation in the coatings.

The difference between the behavior of samples T and TT is reflected in a change of ΔE of approximately 1 point. Since the literature defines a value of ΔE ≥ 1 as necessary to be appreciated by the human eye, it can be stated that samples T and TT exhibit comparable visual and thermochromic characteristics.

Ultimately, the thermochromic pigment, well distributed in the polymeric matrix of the top-coat, provides the samples with an intense color, as well as aesthetic and functional features, responsive to a specific thermal stimulus.

3.3. Coatings protective properties

The protective properties of the paints were studied through Electrochemical Impedance Spectroscopy (EIS) measurements. The Bode impedance module at low frequency (10^{-2} Hz), $|Z|_{(0.01)}$, was monitored for one week, and its evolution is shown in Fig. 7. All three samples show $|Z|_{(0.01)}$ values higher than 10^6 Ω·cm^2, which is considered as the threshold value for a coating to be 'protective' [68,69]. While sample T and sample B display a similar trend of $|Z|_{(0.01)}$, sample TT shows much higher $|Z|_{(0.01)}$ values, thanks to the presence of the clearcoat, which causes a substantial increase in the overall thickness of the coating (see Table 2). During the immersion time, a slightly increased in the impedance module $|Z|_{(0.01)}$ was observed for the three samples series. This trend does not represent an improved protection of the coating, but it is likely explained by poor adhesion between the coating and the substrate. As a consequence, the test solution penetrates, and the swelling of the coating results in the increased Bode module. This behavior has been previously discussed in other works [57,70], highlighting the issues related to the waterborne nature of the paint. However, the similar outcome of samples B and T suggests that the thermochromic pigment behaves like a normal pigment for paints, without introducing significant defectiveness in the organic matrix of the coating. Furthermore, the application of a clearcoat in sample TT results in a evident improvement of the protective performance of the coating, which exerts a substantial barrier effect in favor of the metal substrate.

Ultimately, thermochromic pigments can be used as aesthetic

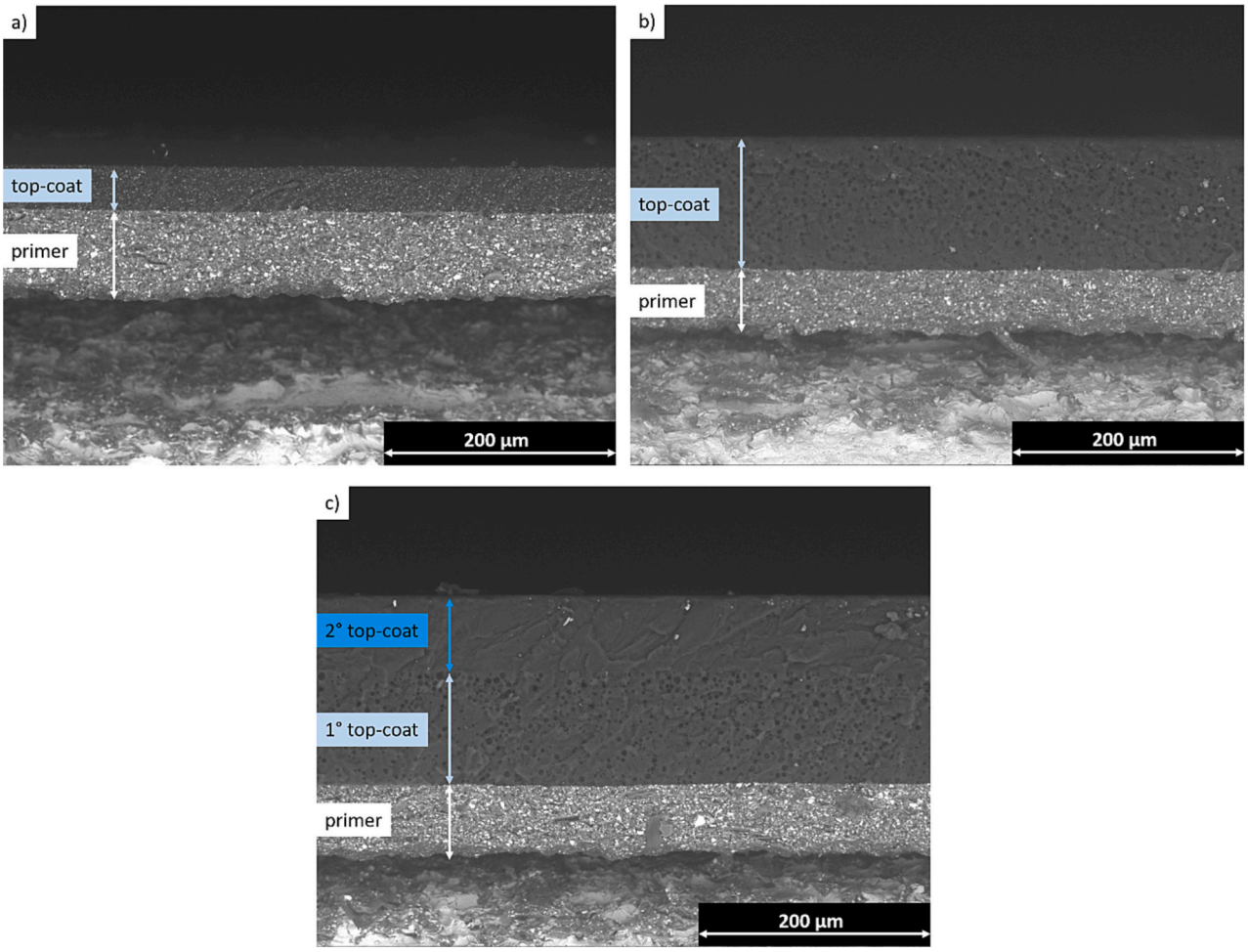

Fig. 5. SEM micrographs of the cross section of (a) sample B, (b) sample T and (c) sample TT.

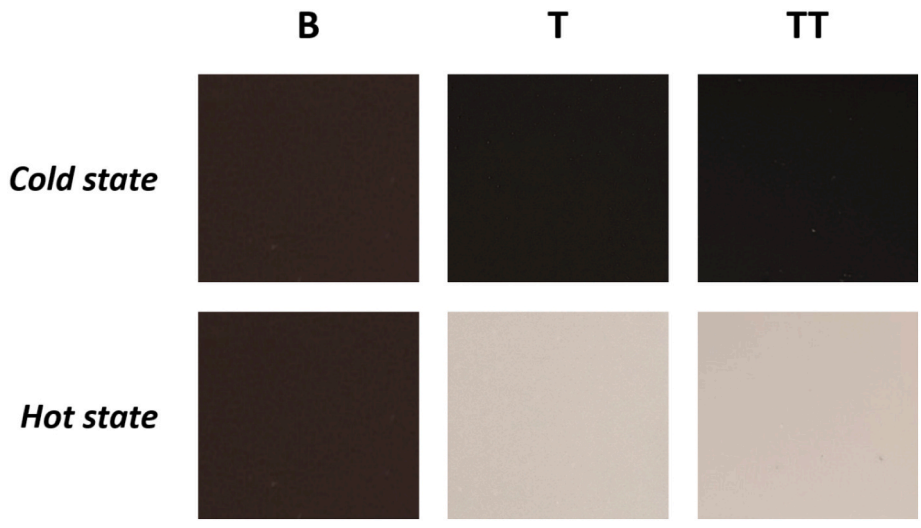

Fig. 6. Photographs of the samples both in cold and hot states.

additives in waterborne paints, as they do not compromise their protective performance. Obviously these protective properties, associated to the barrier performance of the polymer matrix, can be improved simply by increasing the thickness of the coating, by applying multilayers, as in the case of sample TT.

3.4. Coatings durability

3.4.1. Climatic chamber exposure

If the chromogenic coatings are intended for outdoor applications, they are likely to be subjected to continuous temperature fluctuations beneath and above the color transition threshold. Thus, an accelerated

Table 3
Colorimetric coordinates of the samples according to CIEL*a*b*.

Sample	Cold state			Hot state		
	L*	a*	b*	L*	a*	b*
B	27.24	2.36	1.26	27.24	2.36	1.26
T	26.47	1.16	0.04	84.7	0.2	4.56
TT	26.36	1.24	0.03	83.37	0.33	5.05

Table 4
ΔE values of the three series of samples between the cold and hot states.

Sample	B	T	TT
ΔE	/	58.42	57.23

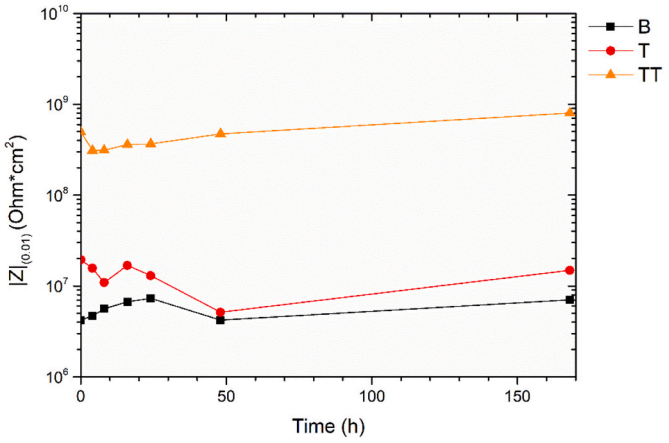

Fig. 7. Bode impedance modulus $|Z|_{(0.01)}$ evolution with time.

test in a climatic chamber was performed, to determine whether the number of temperature fluctuations may negatively affect the thermochromic properties of the coatings. Fig. 8 illustrates the overall color change ΔE observed during the climatic chamber exposure test, relative to the coatings' initial cold and hot states. As expected, sample B revealed high color stability, with no significant color variation. On the other side, higher ΔE values were observed for samples T and TT, suggesting a slight decay of the thermochromic efficiency of the pigments as a result of the continuous thermal shifts. The behavior of the two samples in the cold state is comparable, and is correlated to a limited colorimetric shift (final ΔE ≈ 1), representative of the pigment ability to return to its starting color. Otherwise, the pigments showed a greater color shift in the hot state, associated with a reduction of L* by 1–2 points, as they slightly lose the ability to become completely transparent. This phenomenon is limited in sample TT, with ΔE values varying between 1 and 2 during the test, while it is more evident in sample T, which shows a color shift of 4–5 points. The results suggest that the presence of the clearcoat layer in sample TT increases the durability of the thermochromic pigment. This third polyurethane-acrylate layer is able to protect the delicate spherical structures of the pigment, ensuring its functionality and reversibility even after various changes in temperature.

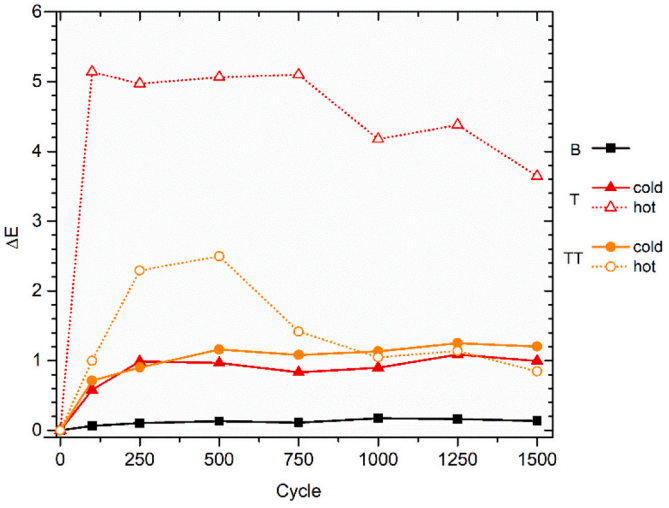

Fig. 8. Total color variation during the climatic chamber exposure test.

Besides the color stability, the other considered parameter during the climatic chamber exposure test is the response time of the total color change, *i.e.*, the time required for the coating for the transition from the colored to the colorless state. Fig. 9 reports the time required for the complete color change, as a function of the number of thermal cycles. Despite the response time necessary for the total color change was measured in the same conditions during the test, some small fluctuations were observed, which may be due to the experimental setup. However, no significant changes in the response time were observed, neither for sample T nor for sample TT. This outcome suggests that the thermochromic properties of the pigment are not affected by the number of times of color transition, and the spherical particles constituting the pigment are still able to change from the color state to the colorless condition.

Ultimately, the thermochromic efficiency of the pigment is ensured over time and its chromatic reversibility is almost complete even after numerous thermal cycles. Although the transparency of the pigment is slightly reduced following sudden changes in temperature, a clearcoat has been shown to be able to limit this phenomenon, ensuring consistent long-term chromatic reversibility to the thermochromic spherules.

3.4.2. *Thermal behavior*

The chromogenic properties of the pigments were also assessed employing a specific degradation test, employing the setup depicted in Fig. 1. Fig. 10 displays the evolution of the plateau temperatures during the degradation test. Sample B sample shows higher temperatures (both T_{ext} and T_{surf}) compared to samples T and TT. In fact, the transparency of the thermochromic pigments above 28 °C reveals the white color of the primer: sample T and sample TT, which are lighter, absorb less energy than the black coating B, with a consequent decrease in the temperature measured on the external surface of the panel (T_{ext}). This phenomenon

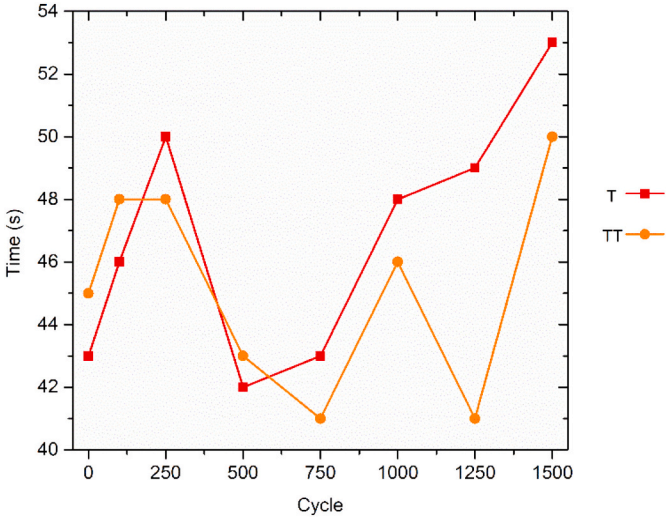

Fig. 9. Response time of the total color change of the samples, as a function of the number of thermal cycles.

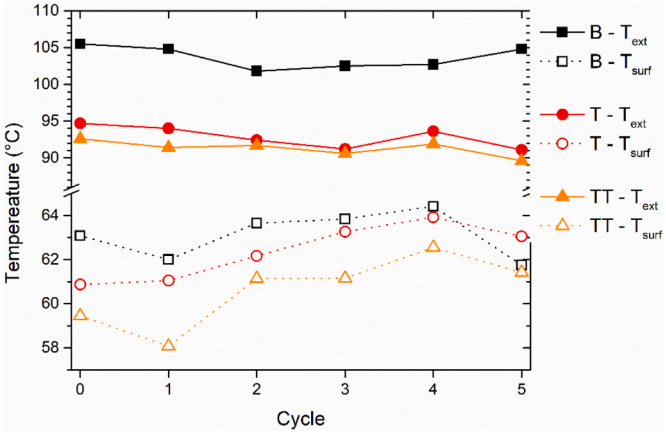

Fig. 10. Coatings thermal behavior.

has also slight repercussions in lower T_{surf} values for the thermochromic coatings.

While the external temperatures of T and TT remained almost unchanged during the degradation test, the surface temperatures display a little increase with the degradation cycles. It should be specified that small changes in the measured temperatures may be caused also by the setup employed in the measurements. However, the temperature values of sample T are tendentially slightly higher than those of the corresponding sample TT. The additional clearcoat of sample TT performs the dual function of protecting the pigment from atmospheric agents and increasing the thickness of the insulating coating against heat flow.

ATR measurements were also performed on each sample series before and after the accelerated degradation test, to identify eventual chemical and structural changes evolved in the coatings. Fig. 11 shows the outcome of the analyses. The presence of the pigments added to the top-coat paint cannot be appreciated by the IR analysis, as their representative peaks are covered by the signal of the polyurethane-acrylate matrix of the transparent top-coat paint. Thus, the ATR spectra for the three sample series are the quite identical. The region between 3400 and 3300 cm^{-1} is related to the NH bond, present in the urea and urethane functional groups. The absorption peaks at 2933 and 2862 cm^{-1} are correlated to the stretching vibration of the CH and of the CH_2 groups. The peak at 1724 cm^{-1} is related to the carbonyl groups, and the peak at 1684 cm^{-1} is due to the stretching vibrations of the urethane and urea carbonyl groups [71]. While the peak at 1528 cm^{-1} is due to the stretching of the NH group [72], the absorption bands at 1460 and 1379 cm^{-1} are typical of the CH_2 aliphatic groups. Moreover, the two peaks at 1238 and 1142 cm^{-1} are due to vibrations of the N—H bond and of the coupled C—N and C—O bonds. The peak at 843 cm^{-1} is attributed to the stretching of the C—H bond, while the intense signal at 764 cm^{-1} corresponds to the symmetric stretching vibrations of the ester bond C-O-C [73].

No evolution of the FTIR spectra was observed during the degradation test. Indeed, the polyurethane-acrylate paint is highly resistant to exposure to UV radiation [74] and, as the pigment is not detected by the IR analysis, the spectra remained reasonably unchanged after the degradation cycles.

Thus, the three sample typologies seem to be highly resistant to degradation based on UV-A/salt spray exposure. However, colorimetric analyses performed after each degradation cycle revealed changes in the appearance of the samples during the test. Fig. 12 reports the total color variation ΔE during the accelerated degradation test, both in the cold state and in the hot state. Coating B showed high color stability, with ΔE values close to 0. Differently, the color of samples T and TT resulted to be significantly affected by the degradation test. In the cold state, the two samples exhibited a continuous increase in color change, with a very similar trend. However, the intensity of this color variation is reduced in sample TT. The color variations are even more evident in the hot state, but also in this case sample TT revealed greater stability, while sample T showed a rapid aesthetic change. The two samples exhibited same values of ΔE only after the fourth degradation cycle. These results indicate that the presence of the clearcoat layer in sample TT improves the wheatering stability of chromogenic properties of the coating, protecting the pigment from degradation due to exposure to UV-A radiation [75] and salt spray solution and promoting its long-term durability.

To determine the effect of the UV radiation on the chromogenic pigment, the spherules were exposed for 100 h to UV-A rays. Fig. 13a and Fig. 13b show the SEM and the stereomicroscope micrograph of the thermochromic pigments in the cold state after the UV-A exposure, respectively. The SEM observation (Fig. 13a) evidenced a partial degradation of the spherical structures of the pigments: the comparison with the spherules of the pigment before exposure to UV-rays (Fig. 2) highlights a structural change, associated with holes in the spheres which should contain ad protect the three thermochromic components. A similar phenomenon has already been analyzed in a previous work [49], which demonstrated the poor durability of this type of pigment when exposed to UV radiation. This physical degradation of the spherical structures affects the thermochromic functionality of the pigment, as shown in Fig. 13b. The image acquired with the optical stereomicroscope after exposure to the UV-A radiation shows the appearance of the pigment in the cold state. If compared with the intact pigment shown in Fig. 3, the powder in Fig. 13b reveals a chemical-physical

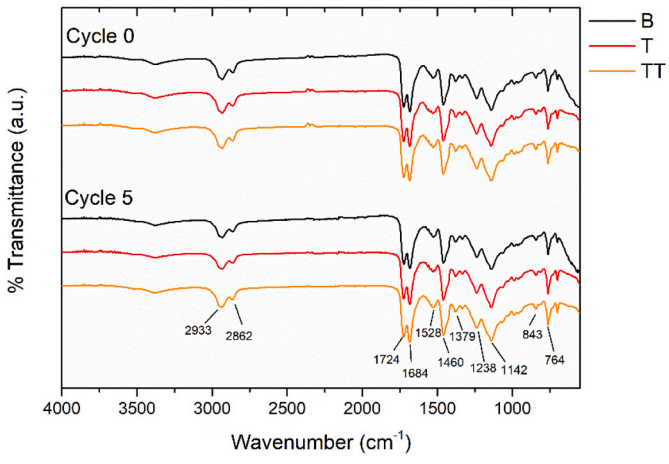

Fig. 11. Evolution of the FTIR spectra of the samples before and after 5 degradation cycles.

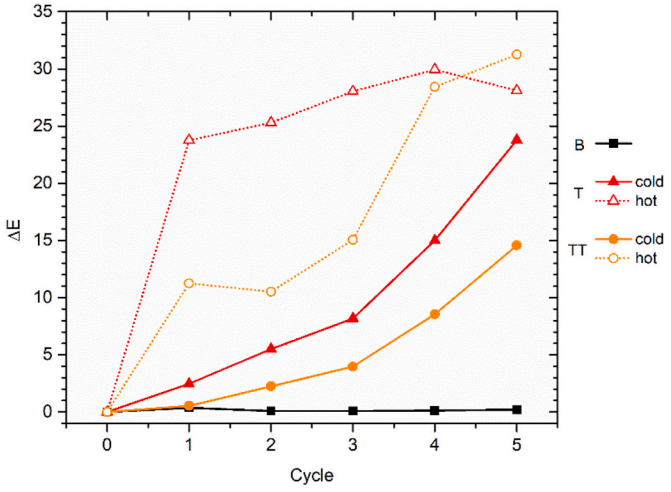

Fig. 12. Total color variation during the accelerated degradation test.

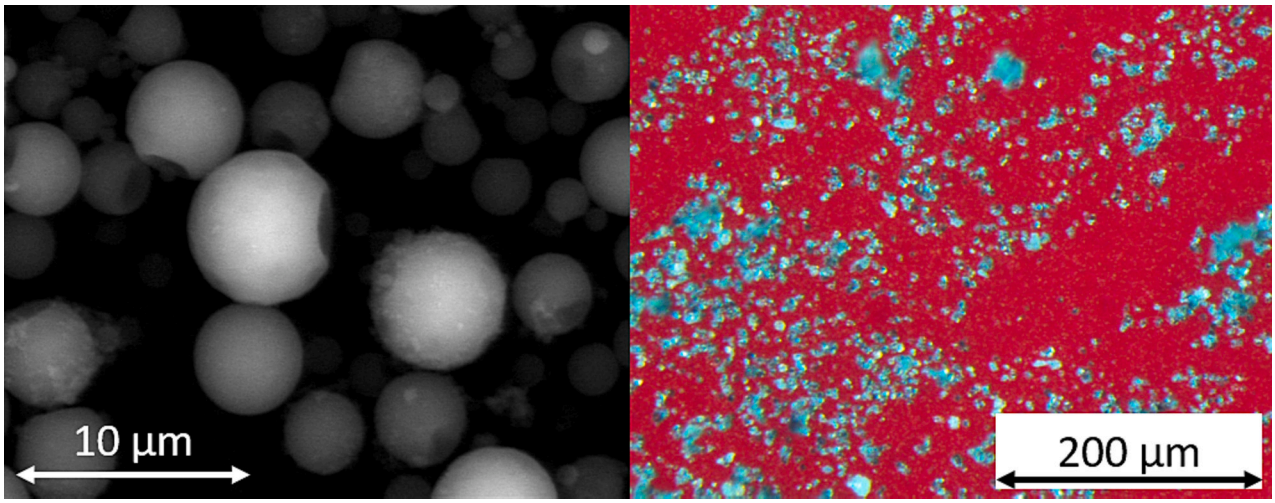

Fig. 13. Thermochromic pigment after 100 h of UV-A exposure observed at SEM (on the left) and optical stereomicroscope (on the right) in the cold state.

degradation, as it is no longer able to return completely black below the transition temperature. As the pigment black coloring is determined by the spherical particles, their breakup induced by the UV radiation involves the loss of the three thermochromic components, with consequent reduction of the black coloring of the pigments.

To quantitatively evaluate their degradation, the pigments were placed on the single white primer, taken as a reference, and subjected to colorimetric measurements. The color coordinates of the primer are the following: L* = 94.3, a* = −0.8, and b* = 1.5. Table 5 reports the difference between the color parameters of the pigment and the white primer, both in cold and hot conditions. Before undergoing degradation, the pigment in the cold state was very dark, and consequently the ΔE compared to the white primer reached high values, exceeding 67 points. Once the threshold temperature of 28 °C was exceeded, the pigments became transparent and revealed the color of the white substrate. However, the ΔE value with respect to the primer is not negligible, but is around 10 points, to represent the incomplete transparency of the pigment. In fact, the brightness of the pigment (L*) is about 10 points lower than that of the white primer. Consequently, these pigments possess a limitation in their thermochromic efficiency and in their ability to become completely transparent.

However, following exposure in the UV-A chamber, the pigment degradation was evidenced by the colorimetric measurements. Indeed, the values of ΔE decrease in the cold state and increase in the hot state, revealing a clear departure from the aesthetic features expressed before the degradation test. In the cold state the pigments appear less dark, while they lose their transparent efficiency in the hot state.

Consequently, the physical degradation of the spherules highlighted in Fig. 13 has repercussions on the thermochromic performance of the pigment in both thermal states. This loss of thermochromic efficiency explains the different thermal behavior of the samples during the degradation test, as well as the evolution of the color change highlighted in Fig. 12. In general, the performance of sample TT is better than that of sample T, thanks to the presence of the clearcoat which acts as a protective film for the thermochromic pigments. By reducing the phenomena of pigment degradation, sample TT is able to exhibit greater thermochromic activity over time, which translates into better thermal performance.

Table 5
Color difference of the pigment with respect to the white layer in the cold and hot states, both before and after the degradation test.

	Cold state (with respect to white primer)				Hot state (with respect to white primer)			
	ΔL	Δa	Δb	ΔE	ΔL	Δa	Δb	ΔE
Before degradation	−67.8	1.9	1.6	67.8	−9.6	1.0	3.1	10.1
After degradation	−46.6	6.0	8.3	47.7	−29.5	8.3	21.5	37.4

3.4.3. *Effect of soiling and weathering*

Fig. 14 summarizes the evolution of the external and superficial temperatures, recorded after 20 min of exposure under IR lamps, *i.e.*, when the plateau is reached. The soiling accelerated test does not seem to affect the samples thermal properties. Indeed, no significant changes in the plateau temperatures were observed. As expected, sample B shows higher plateau temperatures respect to samples T and TT, while similar temperatures were recorded for the two thermochromic coatings. Small fluctuations in the thermic measurements may be due to small variations of the testing conditions, associated with the experimental setup.

After 6 cycles of soiling and weathering, color measurements were performed, both in the hot and cold states. The color was measured both on the soiled samples and on the samples after removal of the soiling mixture with water. The ΔE values with reference to the initial cold and hot state of the samples, both before and after removal of the soiling mixture with water, are reported in Table 6. If the color of sample B was not affected by the test, the same is not true for the other two sample typologies. In the cold state sample TT reveals a much reduced color

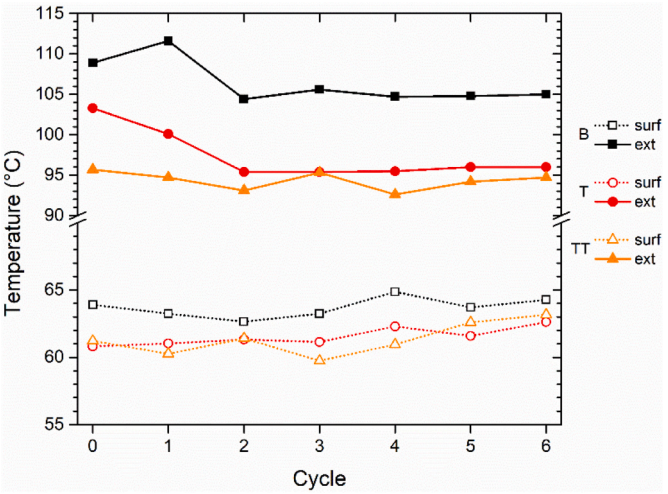

Fig. 14. Temperature evolution during the soiling test.

Table 6
ΔE values of the three series of samples after the soling test.

Sample	Cold state		Hot state	
	ΔE soiled	ΔE clean	ΔE soiled	ΔE clean
B	2.42	0.22	2.42	0.22
T	14.19	14.51	25.85	23.98
TT	4.53	3.95	23.63	22.10

variation than sample T. Thus, these results provide a further confirmation of the protective role of the additional clearcoat layer of sample TT, which increases the durability of the thermochromic coating, preventing its degradation due to exposure to aggressive conditions. The behavior of the two thermochromic coatings is instead similar in the hot state, since the degradation of the pigments mainly involves their difficulty in returning to their natural color in the cold state, acting less on their transparency features. This phenomenon has already been extensively investigated in previous literature studies [49,51]. Therefore, even a limited degradation such as that which occurs in sample TT results in a significant color change in the hot state, similar to that observed in sample T. Consequently, the thermal performances in the hot state of the two thermochromic samples are very similar, as shown in Fig. 14.

However, despite the degradation undergone by the thermochromic pigments and their relative loss of transparency, the temperatures measured in proximity of sample B are always higher, as the coating always appears much darker than that of the two thermochromic coatings. Ultimately, regardless of the type of accelerated degradation test, the presence of the protective layer in the TT sample results in better thermal performance over time.

4. Conclusions

This work has the purpose of optimizing the deposition of thermochromic coatings, improving their durability and long-term efficiency. The thermochromic features of the coatings have been introduced by specific pigments, which demonstrated excellent compatibility with the organic matrix of the layer. These pigments revealed excellent coloring power, as well as high responsibility to thermal stimuli.

The thermochromic pigments did not compromise the protective performance of the coating, as assessed with EIS measurements. The investigations highlighted the useful contribution of the additional clearcoat layer of sample TT, which shows an increased barrier effect against the absorption of aggressive solutions and ions.

The exposure of the pigments to several thermal cycles confirmed their highly thermochromic efficiency and good chromatic reversibility. The clearcoat of samples TT adequately protected the pigments, ensuring also consistent long-term chromatic reversibility to the thermochromic spherules.

The exposure of the samples to accelerated degradation test revealed physical degradation of the spherules, with consequent reduction of their thermochromic performance in both thermal states. This phenomenon not only has consequences on the aesthetics of the samples, but also on their thermal performance as roof-coatings. However, the pigment decay may be limited by the clearcoat layer of sample TT, which exhibited improved thermochromic activity over time, which translated into better thermal performance.

Ultimately, the thermochromic pigments underwent to degradation phenomena also as a result of the Soiling and Weathering test, associated to loss of transparency. Again, the additional clearcoat layer of sample TT demonstrated to be able to reduce the physical decay of the pigment, ensuring better thermal performance over time.

In conclusion, thermochromic pigments are quite delicate materials, whose outdoor applications are limited by a poor durability to external agents. However, a specific design of the coating, composed of an additional protective layer, enables their use in roof-coating applications, the purpose of which is the reduction of heat absorption inside housing structures. Clearly, further efforts could be focused on the synthesis of UV-shielding additives to be incorporated in the clearcoat. This approach would serve to enhance the thermochromic durability of the coating.

CRediT authorship contribution statement

Massimo Calovi: Conceptualization, Methodology, Validation, Investigation, Data curation, Writing – original draft, Writing – review & editing. **Alessia Zanardi:** Methodology, Validation, Investigation, Data curation, Writing – original draft. **Stefano Rossi:** Resources, Writing – review & editing, Supervision, Project administration.

Declaration of competing interest

The authors declare that they have no known competing financial interests or personal relationships

that could have appeared to influence the work reported in this paper.

Data availability

Data will be made available on request.

Acknowledgments

The authors greatly acknowledge Francesco Giubilini (EP vernici s.r.l., Solarolo, Italy) for the paint supply. The publication was created with the co-financing of the European Union – FSE-REACT-EU, PON Research and Innovation 2014-2020 DM1062/2021.

References

[1] World Energy Consumption Statistics | Enerdata. https://yearbook.enerdata.net/total-energy/world-consumption-statistics.html (accessed 2023-05-12).
[2] T. Kober, H.-W. Schiffer, M. Densing, E. Panos, Global energy perspectives to 2060–WEC's world energy scenarios 2019, Energ. Strat. Rev. 31 (2020), 100523.
[3] M. González-Torres, L. Pérez-Lombard, J.F. Coronel, I.R. Maestre, D. Yan, A review on buildings energy information: trends, end-uses, fuels and drivers, Energy Rep. 8 (2022) 626–637.
[4] E.E. Commission, Regulation (EU), 2021/1119 of the European Parliament and of the Council of 30 June 2021 establishing the framework for achieving climate neutrality and amending Regulations (EC) No 401/2009 and (EU) 2018/1999 ('European Climate Law'), document 32021R1119, Off. J. Eur. Union 243 (2021) 1–17.
[5] K.M. Al-Obaidi, M. Ismail, A.M.A. Rahman, Passive cooling techniques through reflective and radiative roofs in tropical houses in Southeast Asia: a literature review, Front. Architect. Res. 3 (2014) 283–297.
[6] D. Kalús, P. Janík, M. Kubica, Experimental house EB2020–research and experimental measurements of an energy roof, Energ. Buildings 248 (2021), 111172.
[7] S. Chen, B.J. Dewancker, S. Yang, J. Mao, J. Chen, Study on the roof solar heating storage system of traditional residences in southern Shaanxi, China, Int. J. Environ. Res. Public Health 18 (2021) 12600.
[8] W. Athmani, L. Sriti, M. Dabaieh, Z. Younsi, The potential of using passive cooling roof techniques to improve thermal performance and energy efficiency of residential buildings in hot arid regions, Buildings 13 (2022) 21.
[9] I.H. Lubis, M.D. Koerniawan, Reducing heat gains and cooling loads through roof structure configurations of a house in Medan, in: IOP Conference Series: Earth and Environmental Science, IOP Publishing, 2018, p. 012008.
[10] J. Feng, S. Haddad, K. Gao, S. Garshasbi, G. Ulpiani, M. Santamouris, G. Ranzi, C. Bartesaghi-Koc, Fighting urban climate change—state of the art of mitigation technologies, Urban Climate Change and Heat Islands (2023) 227–296.
[11] M.A.C. Stuart, W.T. Huck, J. Genzer, M. Müller, C. Ober, M. Stamm, G. B. Sukhorukov, I. Szleifer, V.V. Tsukruk, M. Urban, Emerging applications of stimuli-responsive polymer materials, Nat. Mater. 9 (2010) 101–113.
[12] M. Mrinalini, S. Prasanthkumar, Recent advances on stimuli-responsive smart materials and their applications, ChemPlusChem 84 (2019) 1103–1121.
[13] A.S. Hoffman, The origins and evolution of "controlled" drug delivery systems, J. Control. Release 132 (2008) 153–163.
[14] Y. Yang, W. Zeng, P. Huang, X. Zeng, L. Mei, Smart materials for drug delivery and cancer therapy, View 2 (2021) 20200042.
[15] Z. Mazidi, S. Javanmardi, S.M. Naghib, Z. Mohammadpour, Smart stimuli-responsive implantable drug delivery systems for programmed and on-demand

cancer treatment: an overview on the emerging materials, Chem. Eng. J. 134569 (2022).
[16] M. Su, L. Ruan, X. Dong, S. Tian, W. Lang, M. Wu, Y. Chen, Q. Lv, L. Lei, Current state of knowledge on intelligent-response biological and other macromolecular hydrogels in biomedical engineering: a review, Int. J. Biol. Macromol. 227 (2022) 472–492.
[17] C. Fernandes, G.B. Heggannavar, M.Y. Kariduraganavar, G.R. Mitchell, N. Alves, P. Morouço, Smart materials for biomedical applications: the usefulness of shape-memory polymers, Appl. Mech. Mater. 890 (2019) 237–247.
[18] H. Huangfu, X. Guo, N. Li, Y. Xiong, Y. Huang, J. Zhang, L. Wang, A smart composite coating with self-reporting and self-healing functions to enhance corrosion protection for magnesium alloys, Prog. Org. Coat. 181 (2023), 107598.
[19] S.B. Ulaeto, R. Rajan, J.K. Pancrecious, T. Rajan, B. Pai, Developments in smart anticorrosive coatings with multifunctional characteristics, Prog. Org. Coat. 111 (2017) 294–314.
[20] Z. Tatíčková, J. Kudláček, M. Zoubek, J. Kuchař, Behaviour of Thermochromic coatings under thermal exposure, Coatings 13 (2023) 642.
[21] M. Bengisu, M. Ferrara, Materials that Change Color: Smart Materials, Intelligent Design, 1st ed., Springer, Berlin, Germany, 2014.
[22] W. Zhang, A.P. Schenning, A.J. Kragt, G. Zhou, L.T. De Haan, Reversible thermochromic photonic coatings with a protective topcoat, ACS Appl. Mater. Interfaces 13 (2021) 3153–3160.
[23] J.H. Day, Thermochromism, Chem. Rev. 63 (1963) 65–80.
[24] N. Carmona, E. Herrero-Hernandez, J. Llopis, M. Villegas, Novel sol–gel reversible thermochromic materials for environmental sensors, J. Sol-Gel Sci. Technol. 47 (2008) 31–37.
[25] J. Heiras, E. Pichardo, A. Mahmood, T. López, R. Pérez-Salas, J. Siqueiros, O. Blanco, M. Castellanos, Thermochromism in (Ba, Sr)-Mn oxides, J. Phys. Chem. Solids 63 (2002) 591–595.
[26] J.A. Compton, The thermochromic properties of the ceramic colour standards, Color. Res. Appl. 9 (1984) 15–22.
[27] W. Jeong, M.I. Khazi, D.H. Park, Y.S. Jung, J.M. Kim, Full color light responsive diarylethene inks for reusable paper, Adv. Funct. Mater. 26 (2016) 5230–5238.
[28] D.C. MacLaren, M.A. White, Dye–developer interactions in the crystal violet lactone–lauryl gallate binary system: implications for thermochromism, J. Mater. Chem. 13 (2003) 1695–1700.
[29] R. Kulčar, M. Friškovec, N. Hauptman, A. Vesel, M.K. Gunde, Colorimetric properties of reversible thermochromic printing inks, Dyes Pigments 86 (2010) 271–277.
[30] W. Zhang, X. Ji, C. Zeng, K. Chen, Y. Yin, C. Wang, A new approach for the preparation of durable and reversible color changing polyester fabrics using thermochromic leuco dye-loaded silica nanocapsules, J. Mater. Chem. C 5 (2017) 8169–8178.
[31] Y. Wang, J. Ren, C. Ye, Y. Pei, S. Ling, Thermochromic silks for temperature management and dynamic textile displays, Nano-Micro Letters 13 (2021) 1–17.
[32] M.A. Chowdhury, B.S. Butola, M. Joshi, Application of thermochromic colorants on textiles: temperature dependence of colorimetric properties, Color. Technol. 129 (2013) 232–237.
[33] E. Thamrin, E. Warsiki, Y. Bindar, I. Kartika, Thermochromic ink as a smart indicator on cold product packaging-review, in: IOP Conference Series: Earth and Environmental Science, IOP Publishing, 2022, p. 012021.
[34] S. Rossi, M. Simeoni, A. Quaranta, Behavior of chromogenic pigments and influence of binder in organic smart coatings, Dyes Pigments 184 (2021), 108879.
[35] O. Lima, P. Cardoso, I.R. Segundo, E. Freitas, M.F. Costa, H. Nascimento, C. Afonso, S. Landi, V. Teixeira, J. Carneiro, Thermochromism applied to transportation engineering: asphalt roads and paints, in: Journal of Physics: Conference Series, IOP Publishing, 2022, p. 012042.
[36] J. Hu, X. Yu, Innovative thermochromic asphalt coating: characterisation and thermal performance, Road Mater. Pave. Des. 17 (2016) 187–202.
[37] Y. Zhao, H. Ji, M. Lu, J. Tao, Y. Ou, Y. Wang, Y. Chen, Y. Huang, J. Wang, Y. Mao, Thermochromic smart windows assisted by photothermal nanomaterials, Nanomaterials 12 (2022) 3865.
[38] M. Aburas, V. Soebarto, T. Williamson, R. Liang, H. Ebendorff-Heidepriem, Y. Wu, Thermochromic smart window technologies for building application: a review, Appl. Energy 255 (2019), 113522.
[39] Y. Cui, Y. Ke, C. Liu, Z. Chen, N. Wang, L. Zhang, Y. Long, Thermochromic VO2 for energy-efficient smart windows, Joule 2 (2018) 1707–1746.
[40] J. Hu, X.B. Yu, Adaptive thermochromic roof system: assessment of performance under different climates, Energ. Buildings 192 (2019) 1–14.
[41] T. Karlessi, M. Santamouris, K. Apostolakis, A. Synnefa, I. Livada, Development and testing of thermochromic coatings for buildings and urban structures, Sol. Energy 83 (2009) 538–551.
[42] V. Granadeiro, M. Almeida, T. Souto, V. Leal, J. Machado, A. Mendes, Thermochromic paints on external surfaces: impact assessment for a residential building through thermal and energy simulation, Energies 13 (2020) 1912.
[43] A. Hakami, S.S. Srinivasan, P.K. Biswas, A. Krishnegowda, S.L. Wallen, E. K. Stefanakos, Review on thermochromic materials: development, characterization, and applications, J. Coat. Technol. Res. 19 (2022) 377–402.
[44] C. Fabiani, A.L. Pisello, E. Bou-Zeid, J. Yang, F. Cotana, Adaptive measures for mitigating urban heat islands: the potential of thermochromic materials to control roofing energy balance, Appl. Energy 247 (2019) 155–170.
[45] S. Liu, Z. Liu, J. Wang, X. Ding, X. Meng, Effect of the material color on optical properties of thermochromic coatings employed in buildings, Case Stud. Thermal Eng. 45 (2023), 102916.
[46] C. Fabiani, V. Castaldo, A. Pisello, Thermochromic materials for indoor thermal comfort improvement: finite difference modeling and validation in a real case-study building, Appl. Energy 262 (2020), 114147.
[47] J. Hu, X. Yu, Thermo and light-responsive building envelope: energy analysis under different climate conditions, Sol. Energy 193 (2019) 866–877.
[48] E. Crespo Sánchez, D. Masip Vilà, Thermochromic materials as passive roof technology: their impact on building energy performance, Energies 15 (2022) 2161.
[49] M. Calovi, F. Russo, S. Rossi, Synergic behavior of graphene-based filler and thermochromic pigments in cataphoretic coatings, Prog. Org. Coat. 150 (2021), 105978.
[50] R. Kantola, L.V. Lassila, M. Tolvanen, P.K. Valittu, Color stability of thermochromic pigment in maxillofacial silicone, J. Adv. Prosthodontics 5 (2013) 75–83.
[51] M. Calovi, F. Russo, S. Rossi, Esthetic performance of thermochromic pigments in cataphoretic and sprayed coatings for outdoor applications, J. Appl. Polym. Sci. 138 (2021) 50622.
[52] T. Karlessi, M. Santamouris, Improving the performance of thermochromic coatings with the use of UV and optical filters tested under accelerated aging conditions, Int. J. Low-Carbon Technol. 10 (2015) 45–61.
[53] P. Berdahl, H. Akbari, R. Levinson, W.A. Miller, Weathering of roofing materials–an overview, Constr. Build. Mater. 22 (2008) 423–433.
[54] S. Zhou, Y. Ding, Z. Wang, J. Dong, A. She, Y. Wei, R. Li, Weathering of roofing insulation materials under multi-field coupling conditions, Materials 12 (2019) 3348.
[55] S. Rossi, M. Calovi, D. Dalpiaz, M. Fedel, The influence of NIR pigments on coil coatings' thermal behaviors, Coatings 10 (2020) 514.
[56] M. Calovi, S. Rossi, From wood waste to wood protection: new application of black bio renewable water-based dispersions as pigment for bio-based wood paint, Prog. Org. Coat. 180 (2023), 107577.
[57] M. Calovi, S. Rossi, Durability and thermal behavior of functional paints formulated with recycled-glass hollow microspheres of different size, Materials 16 (2023) 2678.
[58] C. Fabiani, A.L. Pisello, Effect of thermochromic coatings on the indoor thermal behavior of a case study building, in: E3S Web of Conferences, EDP Sciences, 2021, p. 06003.
[59] ISO 20340:2009, Paints and Varnishes - Performance Requirements for Protective Paint Systems for Offshore and Related Structures, ISO - International Organization for Standardization, Geneva, Switzerland, 2009, pp. 1–23.
[60] ISO 11507, Paints and Varnishes - Exposure of Coatings to Artificial Weathering - Exposure to Fluorescent UV and Water 1997, ISO - International Organization for Standardization, Geneva, Switzerland, 1997, pp. 1–9.
[61] ISO 7253, Paints and Varnishes - Determination of Resistance to Neutral Salt Spray (Fog) 1996, ISO - International Organization for Standardization, Geneva, Switzerland, 1996, pp. 1–10.
[62] ASTM D7897–18 - Standard Practice for Laboratory Soiling and Weathering of Roofing Materials to Simulate Effects of Natural Exposure on Solar Reflectance and Thermal Emittance, ASTM International, West Conshohocken (PA), 2018, pp. 1–10.
[63] P. Talvenmaa, Intelligent Textiles and Clothing, 1st ed., Woodhead Publishing Ltd, Cambridge, UK, 2006.
[64] F. Fu, L. Hu, Temperature sensitive colour-changed composites, in: Advanced High Strength Natural Fibre Composites in Construction, Elsevier, 2017, pp. 405–423.
[65] R.S. Hunter, R.W. Harold, The Measurement of Appearance, 2nd ed., John Wiley & Sons, Hoboken, NJ, USA, 1987.
[66] ASTM-E308-18, Standard Practice for Computing the Colors of Objectives by Using the CIE System, West Conshohocken, ASTM International, PA, 2018, pp. 1–45.
[67] E. Carter, Y. Ohno, M. Pointer, A. Robertson, R. Séve, J. Schanda, K. Witt, CIE. Technical Report Colorimetry, 3rd ed, Commission Internationale de l'Eclairage, Vienna, Austria, 2004.
[68] E. Akbarinezhad, M. Bahremandi, H. Faridi, F. Rezaei, Another approach for ranking and evaluating organic paint coatings via electrochemical impedance spectroscopy, Corros. Sci. 51 (2009) 356–363.
[69] A. Amirudin, D. Thieny, Application of electrochemical impedance spectroscopy to study the degradation of polymer-coated metals, Prog. Org. Coat. 26 (1995) 1–28.
[70] M. Calovi, S. Rossi, Functional olive pit powders: the role of the bio-based filler in reducing the water uptake phenomena of the waterborne paint, Coatings 13 (2023) 442.
[71] D. Kunwong, N. Sumanochitraporn, S. Kaewpirom, Curing behavior of a UV-curable coating based on urethane acrylate oligomer: the influence of reactive monomers, Songklanakarin J. Sci. Technol. 33 (2011) 201.
[72] A. Bahadur, M. Shoaib, A. Saeed, S. Iqbal, FT-IR spectroscopic and thermal study of waterborne polyurethane-acrylate leather coatings using tartaric acid as an ionomer, e-Polymers 16 (2016) 463–474.
[73] G. Mashouf, M. Ebrahimi, S. Bastani, UV curable urethane acrylate coatings formulation: experimental design approach, Pigm. Resin Technol. 43 (2014) 61–68.
[74] M. Calovi, S. Rossi, Olive pit powder as multifunctional pigment for waterborne paint: influence of the bio-based filler on the aesthetics, durability and mechanical features of the polymer matrix, Ind. Crop. Prod. 194 (2023), 116326.
[75] F. Lopes, J. Neves, A. Campos, R. Hrdina, Weathering of microencapsulated thermochromic pigments, Res. J. Text. Appar. 13 (2009) 78.